Processes and products of turbidity currents entering soft muddy substrates

Jaco H. Baas[1], Rafael Manica[2], Eduardo Puhl[2], Iris Verhagen[1], and Ana Luiza de O. Borges[2]
[1]School of Ocean Sciences, Bangor University, Menai Bridge, Ynys Môn LL59 5AB, UK
[2]NECOD, Hydrology and Hydromechanics Department, Hydraulics Research Institute, Federal University of Rio Grande do Sul, Avenida Bento Gonçalves 9500, 91501-970, Porto Alegre, Brazil

ABSTRACT

New laboratory experiments reveal that cohesionless turbidity currents are able to enter cohesive soft muddy substrates without losing their shape. These intrabed currents are driven by bed shear stress exceeding bed cohesive strength, and by flow density exceeding bed density. The flows produce unique turbidites with internal mud layers, mixed cohesive-noncohesive sediment layers, and flame and load structures. A depositional model for intrabed (I) turbidites is proposed, comprising, from base to top: I1—sand-bearing mud, with a scoured base, dispersed mud, and mud clasts; I2—muddy sand from the intrabed portion of the turbidity current; I3—sandy mud with a speckled appearance; and I4—mud-poor sand from the suprabed portion of the flow. Complete I1–I4 turbidites are inferred to dominate locations in nature where the currents mix with the bed and deep erosional scours form, filled with deformed or chaotic sand-mud mixtures. Further downflow, base-missing I2–I4 and I4 sequences signify gradual deceleration, loss of erosivity, and termination of intrabed flow.

INTRODUCTION

Sediment gravity flows in ocean basins drive the largest volumes of sediment transport on Earth; among these, turbidity currents are of great scientific, societal, and economic relevance (Weimer and Link, 1991). Process models for turbidity current deposits (i.e., turbidites) are based on field observations and laboratory and computer simulations (e.g., Postma et al., 1988; Baas et al., 2004; Cantero et al., 2012; Manica, 2012). These simulations typically model fixed or loose sandy substrates. However, many ocean beds are rich in mud-sized sediment (e.g., Fagel, 2007), which, unlike sand, is cohesive and behaves as a deformable fluid at high water content and a firm bed at low water content (Coussot, 1995). The interaction of muddy substrates with the base of turbidity currents therefore depends more on consolidation state than on particle size (Winterwerp, 2002; Amy et al., 2006). Verhagen et al. (2013) described coherent deformation of soft muddy substrates when in contact with turbidity currents; this unique behavior of cohesive beds could explain the genetic origin of turbidites that diverge from classic, sand-prone models (Bouma, 1962). Examples of soft-sediment deformation in mud-rich deposits, such as load and flame structures, convolutions, chaotic mud-sand mixtures, and sediment injections, are numerous in the geological record (e.g., Kawakami and Kawamura, 2002; Puigdefàbregas et al., 2004; Kane, 2010; Owen et al., 2011). Such sedimentary structures produce heterogeneities of economic importance (Scott et al., 2013), thus reinforcing the need to better understand the interaction between flows and muddy beds, and their sedimentary products.

We present experimental evidence of turbidity currents that enter soft muddy substrates. This hitherto unknown intrabed flow is associated with soft-sediment deformation structures that form the basis for a genetic model of intrabed turbidites.

METHODS

Turbidity currents were produced by releasing coal suspensions from an overhead reservoir onto the horizontal bottom of a rectangular channel, which contained a 4.5-m-long, 0.22-m-wide, 0.08-m-deep reservoir filled with soft kaolin clay. The coal and kaolin particles had median grain sizes of 0.055 mm and 0.007 mm and densities of 1190 kg m^{-3} and 2600 kg m^{-3}, respectively. The low density of the coal allowed the experimental flows to be scaled to typically faster prototype flows carrying quartz-rich sand (see the GSA Data Repository[1] for full scaling analysis). Initial flow densities (ρ_f) were 1002, 1010, 1019, 1029, and 1044 kg m^{-3} (Table DR1 in the Data Repository). The mud reservoir was made by settling of kaolin for 0.6 h from a turbidity current that reflected off vertical walls at both ends of the reservoir. This produced a linear vertical density gradient from ~1016 kg m^{-3} at the mud-water interface to ~1096 kg m^{-3} at 0.08 m within the bed. Video cameras recorded flow-bed interactions and depositional processes. Ultrahigh concentration meters (Felix et al., 2005; Manica, 2012) measured suspended sediment concentrations at different levels below and above the bed surface at a horizontal distance $x \approx 3.5$ m from the inlet. An ultrasound scanner recorded the interface between substrate and turbidity current at $x \approx 1.7$ m (Figs. 1C–1E). The flow discharge was 50 L min^{-1} for 75 s in each experiment. The contrasting dark currents and light substrate allowed for easy identification of coal, mud, and mixed sediment in flow and bed (Figs. 1A and 1B). Control experiments were performed using the same flow parameters, but with a fixed, smooth bed to determine how soft muddy beds change flow dynamics.

[1]GSA Data Repository item 2014140, upscaling of experimental to natural turbidity currents, and Table DR1 (experimental parameters), is available online at www.geosociety.org/pubs/ft2014.htm, or on request from editing@geosociety.org or Documents Secretary, GSA, P.O. Box 9140, Boulder, CO 80301, USA.

FLOW-BED INTERACTION

The interaction between the turbidity currents and the muddy substrate varied with initial density and travel distance of the flow. Small interfacial waves and weak erosion changed via pronounced interfacial waves into strong mixing and erosion as flow density was increased (Verhagen et al., 2013). A convex-upward bed pressure wave faced all currents (e.g.,

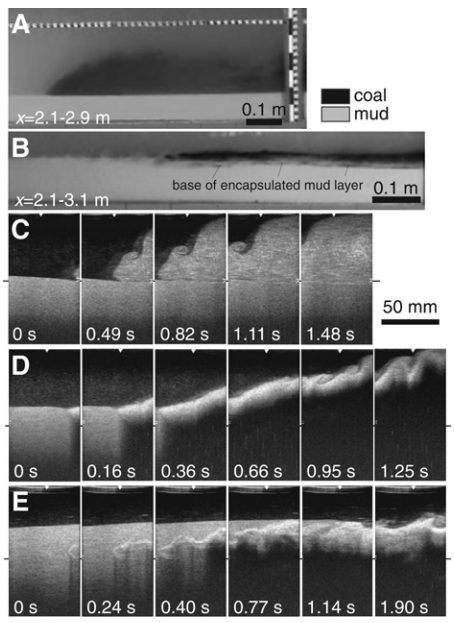

Figure 1. Main properties of experimental turbidity currents. A: Video image of 1002 kg m^{-3} flow (run 1). B: Video image of 1044 kg m^{-3} flow (run 5). Note light mud layer within dark coal flow. C–E: Ultrasound images; black horizontal line is original bed. C: 1002 kg m^{-3} flow (run 1), which moves on top of bed only. D: 1019 kg m^{-3} flow (run 3), where 84% of head moves below bed surface. E: 1044 kg m^{-3} flow (run 5), with top of flow emerging above bed surface after ~1.1 s.

Figs. 1C and 1E). The wave height increased from ~6 mm at ρ_f = 1002 kg m^{-3} (Fig. 1C) to ~37 mm at ρ_f = 1044 kg m^{-3} (Fig. 1E). With increasing flow density, the frontal slope of the currents decreased (cf. Figs. 1A and 1B), and the thickness of the head of the currents above the local bed surface decreased from ~90 to ~25 mm (Figs. 1A and 1B). However, the ultrasound recordings showed that at $\rho_f \geq$ 1010 kg m^{-3}, the currents moved partly below the bed surface (Figs. 1D and 1E). The entire front of the 1029 and 1044 kg m^{-3} flows traveled inside the bed over a length of ~30 mm and ~100 mm, respectively, before emerging above the bed (Figs. 1B and 1E). These remarkable intrabed currents had the same shape as ordinary bottom-hugging turbidity currents, and mixing with the surrounding mud was insufficient to destroy the currents. The 1019 and 1010 kg m^{-3} flows were partly submerged upon arrival at the ultrasound scanner (Fig. 1D). The base of the lowest-density flow was flush with the bed surface (Fig. 1C). Mud was incorporated into the flow at the point of emergence of the intrabed turbidity currents, forming long and persistent, horizontal, coal-bearing, mud layers encapsulated by the intrabed and suprabed flow portions (Fig. 1B). Ultrahigh concentration meter data revealed that intrabed flow portions were denser than surrounding mud, e.g., the basal density of the flow in run 5 (Table DR1) was 1080 ± 60 kg m^{-3}, compared to 1033 kg m^{-3} for the mud facing and overlying this flow. The lowest-density flow showed the lowest density difference: 1016 kg m^{-3} for bed mud versus 1010 ± 10 kg m^{-3} near the flow's base.

The mean head velocity of the turbidity currents increased from ~0.06 m s^{-1} (ρ_f = 1002 kg m^{-3}) to ~0.12 m s^{-1} (ρ_f = 1019 kg m^{-3} and ρ_f = 1029 kg m^{-3}), before decreasing to ~0.11 m s^{-1} (ρ_f = 1044 kg m^{-3}) (Table DR1). In contrast, the head velocity of flows over the fixed, smooth bed increased continuously from ~0.04 to ~0.15 m s^{-1} for the same density range.

The muddy substrate was eroded into scoop-shaped scours near the origin of the flows. The depth of erosion was 50–60 mm at x = 0.6 m; the scours shallowed further downflow. Some eroded mud was transported down the channel in the intrabed portion of the current, but most was mixed locally into the coal as dispersed mud and mud clasts (Fig. 2A).

DEPOSITS OF INTRABED TURBIDITY CURRENTS

The turbidity currents formed deposits that decreased in thickness from several centimeters to millimeters along the flow path (Figs. 2A and 2B). Downflow, the deposits comprised mixed coal-mud covered by mud-poor coal (Fig. 2B). The mud in the lower division originated from advection and minor erosion and mixing with coal during flow. The coal in the upper division settled from suspension after the flow had stopped. Upflow, the deposits were more complex and closely related to flow characteristics and flow-bed interaction. The mud incorporated at the point of emergence of the intrabed turbidity currents was gradually mixed with coal in the body of the flows. However, this encapsulated mud layer was preserved as central divisions of coal-bearing mud in most deposits (Figs. 2D and 2E). The intrabed turbidites (denoted by I) thus consisted of, from base to top: I1—coal-bearing mud, with both dispersed mud and mud clasts and a scoured base, formed by local mixing and erosion; I2—muddy coal, representing the intrabed flow portion; I3—coaly mud with a speckled appearance, representing the encapsulated mud layer; and I4—mud-poor coal, representing the suprabed flow portion and post-flow suspension settling. The I1 division followed by the I2 and I3 divisions pinched out downflow (Fig. 2D), eventually connecting the I4 division to the mud substrate. The 1002 kg m^{-3} flow deposit lacked I2 and I3 divisions. The 1010 kg m^{-3} flow deposit (Fig. 2A) was dominated by mixed sand-mud upflow and lacked distinct I2 and I3 divisions downflow.

Soft-sediment deformation was ubiquitous in all experiments. Load structures (Fig. 2E) separated by small flame structures (Fig. 2F) started growing at the base of the turbidites near the end of the experiments, reaching heights of as much as ~10 mm after the flows had stopped. Mud particles were ejected into the overlying turbidite, forming mud plumes, the mud mostly accumulating at levels similar to those of the encapsulated mud. Some flame structures and overlying mud plumes dipped in the direction of flow (Fig. 2F).

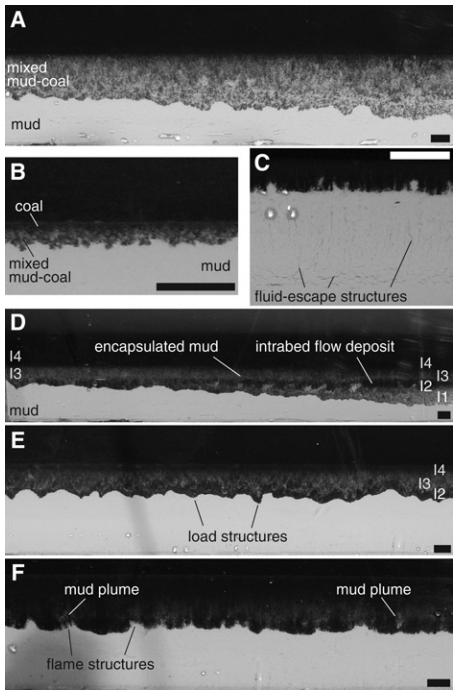

Figure 2. Main properties of experimental turbidites. Flow was from right to left. Scale bar is 20 mm long in all photographs. Coal is black, mud is gray. When photographs were taken, finest coal fraction was still slowly settling out of suspension. A: Coal with dispersed mud and mud clasts deposited on erosional mud surface near origin of flow (flow density, ρ_f, = 1010 kg m^{-3}, run 2). This flow lacked distinct intrabed properties; mud was not as clearly incorporated as in higher density flows, hence no intercalated muddy and sandy sediment layers formed on top of this mixed coal-mud deposit. B: Thin downflow deposit, comprising mixed coal-mud covered by mud-poor coal (ρ_f = 1002 kg m^{-3}, run 1). C: Fluid escape structures supplying flame structures at base of turbidite (ρ_f = 1044 kg m^{-3}, run 5). D: Complete I1–I4 intrabed turbidite sequence (right) evolving to base-missing sequences by progressive pinching out of I1 and I2–I3 divisions (left). Note mud clasts at top of I1 division (ρ_f = 1019 kg m^{-3}, run 3). E: Poorly developed I2–I4 sequence, where loading folded overlying sediment layers (ρ_f = 1010 kg m^{-3}, run 2). F: Flame structures and load structures at base of coal-rich turbidite. Note plumes of mud above flame structures (ρ_f = 1044 kg m^{-3}, run 5).

MODEL FOR INTRABED FLOW DYNAMICS AND DEPOSITIONAL PROCESSES

The experiments confirm that turbidity currents interact differently with soft muddy substrates than with sandy substrates. Unlike sand, clay is able to form a network of cohesive bonds that provides strength to the muddy substrate, such as at the bed densities of 1016–1096 kg m^{-3} used herein (cf. Winterwerp, 2002). The currents need to apply sufficient bed shear stress to overcome this strength to erode the mud. Here, the cohesive structure of the bed was largely retained at low shear, yet the bed deformed coherently, as shown by the interfacial waves below the low-density currents and the bed pressure wave facing all currents (Figs. 1C–1E). At high shear in upflow locations, the bonds between clay particles were partly or fully broken, and the mud was eroded and mixed into the currents either as clasts or in dispersed form, resulting in chaotic mixed mud-coal deposits (Fig. 2A) that showed almost no horizontal movement. This is in agreement with Mitchener and Torfs (1996), in that mixtures of clay and sand are less mobile than their constituents. These deposits should therefore not be mistaken for debrites.

The muddy bed was less dense than the turbidity currents at $\rho_f \geq$ 1010 kg m^{-3}. This explains why these currents entered the substrate and traveled partly or fully inside the substrate for several meters (Fig. 3A). The frontal bed pressure wave might have helped the currents to push into the mud. We infer that the cohesive strength of the mud was high enough to withstand mixing with the intrabed portion of the ≥1029 kg m^{-3} flows. For mud moving over the top of the intrabed currents at ≤0.1 m s^{-1},

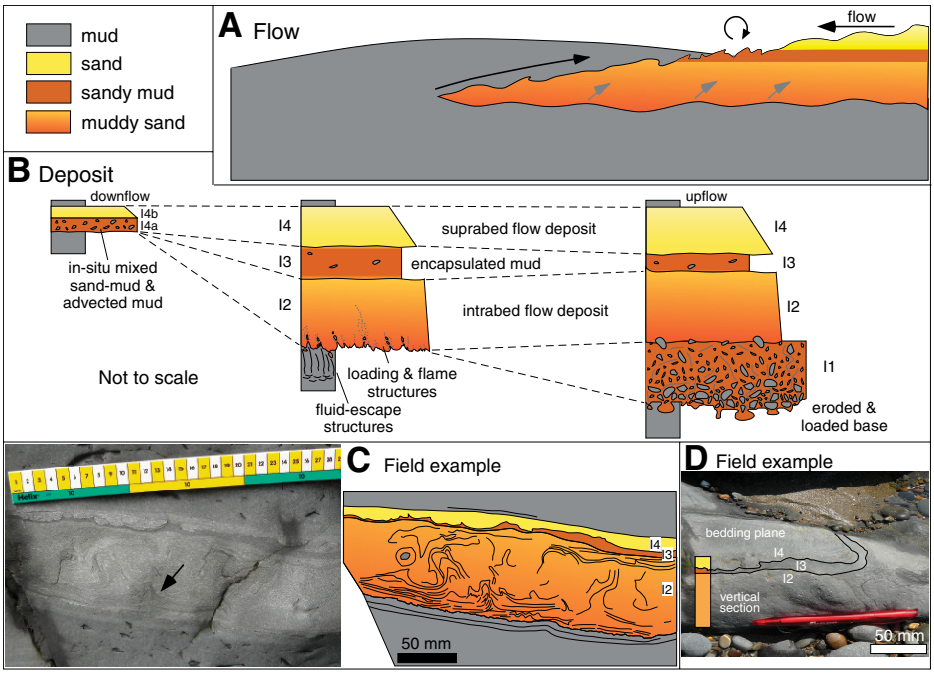

Figure 3. A: Model for intrabed turbidity current dynamics. B: Model for depositional properties. C, D: Field example of I2–I4 sequence in Aberystwyth Grits Formation (Wales, UK, Clarach Bay, 52.4365°N, 4.0826°W). Arrow in C points to mud incorporated into convoluted sand from below. D shows same bed as in C, but 17 m upflow, where I3 division (between thin black lines) bends upward and disappears from bed. Note that D shows vertical section and bedding-plane section of turbidite, so in upper right, I3 division has apparent dip angle that is higher than real dip angle of ~10º.

viscous quasi-laminar flow is predicted (Baas et al., 2009), that should impede mixing at this interface. It is inferred that the mud also kept sufficient strength to withstand mixing after it was incorporated into the current at the point of flow emergence (Fig. 3A), given the preservation of the encapsulated mud layers. The intrabed currents had a smaller density difference with the ambient than the fixed-bed control currents, explaining the lower head velocity at ρ_f = 1044 kg m^{-3}.

A depositional model for intrabed turbidites is proposed in Figure 3B, scaled to deposits that contain natural sand and mud instead of coal and kaolin (see the Data Repository for scaling analysis). Complete I1–I4 sequences prevail in locations where the current enters the bed and deep erosional scours filled with mixtures of sand and mud form. As in the experimental deposits, an encapsulated mud layer (I3 division) separates the intrabed portion (I2 division) from the suprabed portion (I4 division) of the turbidite (Fig. 3B). The I2 division resembles a turbidite with abundant evidence of soft-sediment deformation and horizontal injection. The I4 division resembles a Bouma-type turbidite (Bouma, 1962), with evidence for gradual flow deceleration and suspension settling. In a downflow direction, thinner, base-missing I2–I4 and I4 sequences (Fig. 3B) signify the gradual loss of momentum and erosivity of the turbidity currents, and the termination of intrabed flow, possibly owing to reemergence above the bed surface or immobilization inside the bed. The I4 sequences can be subdivided into a lower mixed sand-mud (I4a) and upper graded sand (I4b; Fig. 3B).

Soft-sediment deformation is inferred to be a strong indicator of flow over soft muddy beds in general and of intrabed flow in particular. Load structures grow at the flow-bed interface from overburden pressure by sediment depositing from the body and tail of the turbidity current. Overburden pressure also induces the generation of fluid-escape structures within the mud, flame structures at the flow-bed interface, and mud plumes within the I1 and I2 divisions.

MODEL APPLICATIONS

Evidence for soft-sediment deformation is widespread in the Silurian deep-marine basin fill of the Aberystwyth Grits Group (Wales, UK; Wood and Smith, 1958), suggesting a soft, muddy basin floor. Figures 3C and 3D show one example of several mixed sandstone-mudstone beds, exposed along Clarach Bay, which are interpreted as I2–I4 intrabed turbidites based on similarities with the intrabed turbidite model, where I2 is a 0.07-m-thick sandstone, with small load and flame structures at its base and pervasive convolute lamination. The convolutions appear to have incorporated soft mud from below in irregular mud patches (see arrow in Fig. 3C) and a few mud clasts as part of the intrabed portion of the turbidity current; I3 is an irregular, <0.01-m-thick, slightly sandy mudstone, interpreted as an encapsulated mud layer, and I4 is a <0.015-m-thick, normally graded sandstone, loaded into the underlying mudstone, suggesting that deposition of sand took place soon after formation of the I2 division within the suprabed portion of the current. This I2–I4 turbidite was traced upflow for 17 m, where the I3 division bends upward at an angle of ~10º (Fig. 3D) to be replaced by a bed consisting entirely of deformed muddy sandstone. We infer that this is the location where the current entered the bed and intrabed flow started.

This turbidite deposit resembles the deposits formed by the experimental, slow-moving, turbidity currents. Further research is needed to determine if and how larger scale flows interact with soft muddy substrates to form decimeter- and meter-scale intrabed turbidites, and how to explain the increasing number of enigmatic hybrid event beds (Haughton et al., 2003; Manica, 2012; Talling et al., 2012) and transitional flow deposits (Baas et al., 2011; Kane and Pontén, 2012) found in deep-marine successions. Such research should rely on the following laboratory-derived constraints for the genesis of intrabed turbidites: (1) presence of stable soft mud; (2) bed shear stress is lower than the critical stress for erosion (cf. Sawyer et al., 2012); and (3) flow density is higher than bed density. The formation and preservation of soft mud are physical processes that are independent of water depth but require dynamic processes that preserve the soft character of the mud and counteract bed compaction. In addition, bed slopes are required that are sufficiently gentle to prevent the mud from moving downslope by gravity (e.g., McAnally et al., 2007). In ocean basins, these conditions are restricted to horizontal or confined basin floors, such as the base of the continental slope and basin plains that undergo frequent stirring by, for example, bottom currents, density currents, storm waves, and seismic shock waves. Typically thick turbiditic mud caps in ponded minibasins might also promote intrabed flow. Constraints 2 and 3 imply that intrabed behavior is not restricted to slow natural turbidity currents, as long as the mud above a fast-moving intrabed flow is strong enough to withstand or decelerate mixing with that flow. The rate of this vertical mixing process, which increases with increasing flow velocity and with decreasing density difference (e.g., Middleton, 1993), should govern the length of the intrabed portion of the turbidity current. Therefore, the distance between the nose of the intrabed flow and the point of reemergence above the substrate should be longer for slow turbidity currents than for fast turbidity currents, but this need not imply that intrabed flow behavior is more common under laboratory conditions, as the effect of faster velocity can be counteracted by a greater density

difference with the overlying mud. Moreover, the strength of cohesive mud increases exponentially with increasing density (e.g., Wan, 1982), implying that, when present, intrabed flow will be more stable than expected solely from density and velocity effects.

ACKNOWLEDGMENTS

We thank the technicians, staff, and students at NECOD (Núcleo de Estudos em Correntes de Densidade, Universidade Federal do Rio Grande do Sul, Brazil) for invaluable assistance (by kind permission from R.D. Maestri), and D. Hodgson, I. Kane, G. Owen, and P. Talling for thoughtful reviews of our work. Petrobras (via A.R. Viana) kindly funded this research.

REFERENCES CITED

Amy, L.A., Talling, P.J., Edmonds, V.O., Sumner, E.J., and Leseur, A., 2006, An experimental investigation on sand-mud suspension settling behaviour and implications for bimodal mud content of submarine flow deposits: Sedimentology, v. 53, p. 1411–1434, doi:10.1111/j.1365-3091.2006.00815.x.

Baas, J.H., Van Kesteren, W., and Postma, G., 2004, Deposits of depletive high-density turbidity currents: A flume analogue of bed geometry, structure and texture: Sedimentology, v. 51, p. 1053–1088, doi:10.1111/j.1365-3091.2004.00660.x.

Baas, J.H., Best, J.L., Peakall, J., and Wang, M., 2009, A phase diagram for turbulent, transitional, and laminar clay suspension flows: Journal of Sedimentary Research, v. 79, p. 162–183, doi:10.2110/jsr.2009.025.

Baas, J.H., Best, J.L., and Peakall, J., 2011, Depositional processes, bedform development and hybrid bed formation in rapidly decelerated cohesive (mud-sand) sediment flows: Sedimentology, v. 58, p. 1953–1987, doi:10.1111/j.1365-3091.2011.01247.x.

Bouma, A.H., 1962, Sedimentology of some flysch deposits: A graphic approach to facies interpretation: Amsterdam, Elsevier, 168 p.

Cantero, M.I., Cantelli, A., Pirmez, C., Balachandar, S., Mohrig, D., Hickson, T.A., Yeh, T.H., Naruse, H., and Parker, G., 2012, Emplacement of massive turbidites linked to extinction of turbulence in turbidity currents: Nature Geoscience, v. 5, p. 42–45, doi:10.1038/ngeo1320.

Coussot, P., 1995, Structural similarity and transitions from Newtonian to non-Newtonian behaviour for clay-water suspensions: Physical Review Letters, v. 74, p. 3971–3974, doi:10.1103/PhysRevLett.74.3971.

Fagel, N., 2007, Clay minerals, deep circulation and climate, *in* Hillaire-Marcel, C., and De Vernal, A., eds., Developments in marine geology, Volume 1: Amsterdam, Elsevier, p. 139–184.

Felix, M., Sturton, S., and Peakall, J., 2005, Combined measurements of velocity and concentration in experimental turbidity currents: Sedimentary Geology, v. 179, p. 31–47, doi:10.1016/j.sedgeo.2005.04.008.

Haughton, P.D.W., Barker, S.P., and McCaffrey, W.M., 2003, Linked debrites in sand-rich turbidite systems—Origin and significance: Sedimentology, v. 50, p. 459–482, doi:10.1046/j.1365-3091.2003.00560.x.

Kane, I.A., 2010, Development and flow structures of sand injectites: The Hind Sandstone Member injectite complex, Carboniferous, UK: Marine and Petroleum Geology, v. 27, p. 1200–1215, doi:10.1016/j.marpetgeo.2010.02.009.

Kane, I.A., and Pontén, A.S.M., 2012, Submarine transitional flow deposits in the Paleogene Gulf of Mexico: Geology, v. 40, p. 1119–1122, doi:10.1130/G33410.1.

Kawakami, G., and Kawamura, M., 2002, Sediment flow and deformation (SFD) layers: Evidence for intrastratal flow in laminated muddy sediments of the Triassic Osawa Formation, northeast Japan: Journal of Sedimentary Research, v. 72, p. 171–181, doi:10.1306/041601720171.

Manica, R., 2012, Sediment gravity flows: Study based on experimental simulations, *in* Schulz, H.E., et al., eds., Hydrodynamics—Natural water bodies: Rijeka, Croatia, InTech, p. 263–286, doi:10.5772/28794.

McAnally, W.H., Friedrichs, C., Hamilton, D., Hayter, E., Shrestha, P., Rodriguez, H., Sheremet, A., and Teeter, A., 2007, Management of fluid mud in estuaries, bays, and lakes: I. Present state of understanding on character and behavior: Journal of Hydraulic Engineering, v. 133, p. 9–22, doi:10.1061/(ASCE)0733-9429(2007)133:1(9).

Middleton, G.V., 1993, Sediment deposition from turbidity currents: Annual Review of Earth and Planetary Sciences, v. 21, p. 89–114, doi:10.1146/annurev.ea.21.050193.000513.

Mitchener, H., and Torfs, H., 1996, Erosion of mud/sand mixtures: Coastal Engineering, v. 29, p. 1–25, doi:10.1016/S0378-3839(96)00002-6.

Owen, G., Moretti, M., and Alfaro, P., 2011, Recognising triggers for soft-sediment deformation: Current understanding and future directions: Sedimentary Geology, v. 235, p. 133–140, doi:10.1016/j.sedgeo.2010.12.010.

Postma, G., Nemec, W., and Kleinspehn, K.L., 1988, Large floating clasts in turbidites: A mechanism for their emplacement: Sedimentary Geology, v. 58, p. 47–61, doi:10.1016/0037-0738(88)90005-X.

Puigdefàbregas, C., Gjelberg, J., and Vaksdal, M., 2004, The Grès d'Annot in the Annot syncline: Outer basin-margin onlap and associated soft-sediment deformation, *in* Joseph, P., and Lomas, A.S., eds., Deep-water sedimentation in the Alpine Foreland Basin of SE France: New perspectives on the Grès d'Annot and related systems: Geological Society of London Special Publication 221, p. 367–388, doi:10.1144/GSL.SP.2004.221.01.20.

Sawyer, D.E., Flemings, P.B., Buttles, J., and Mohrig, D., 2012, Mudflow transport behavior and deposit morphology: Role of shear stress to yield strength ratio in subaqueous experiments: Marine Geology, v. 307–310, p. 28–39, doi:10.1016/j.margeo.2012.01.009.

Scott, A., Hurst, A., and Vigorito, M., 2013, Outcrop-based reservoir characterization of a kilometer-scale sand-injectite complex: American Association of Petroleum Geologists Bulletin, v. 97, p. 309–343, doi:10.1306/05141211184.

Talling, P.J., Masson, D.G., Sumner, E.J., and Malgesini, G., 2012, Subaqueous sediment density flows: Depositional processes and deposit types: Sedimentology, v. 59, p. 1937–2003, doi:10.1111/j.1365-3091.2012.01353.x.

Verhagen, I.T.E., Baas, J.H., Jacinto, R.S., McCaffrey, W.D., and Davies, A.G., 2013, A first classification scheme of flow-bed interaction for clay-laden density currents and soft substrates: Ocean Dynamics, v. 63, p. 385–397, doi:10.1007/s10236-013-0602-8.

Wan, Z., 1982, Bed material movement in hyperconcentrated flow: Institute of Hydrodynamics and Hydraulic Engineering, Technical University of Denmark, Series Paper 31, p. 16–24.

Weimer, P., and Link, M.H., 1991, Global petroleum occurrences in submarine fans and turbidite systems, *in* Weimer, P., and Link, M.H., eds., Seismic facies and sedimentary processes of submarine fans and turbidite systems: New York, Springer-Verlag, p. 9–67.

Winterwerp, J.C., 2002, On the flocculation and settling velocity of estuarine mud: Continental Shelf Research, v. 22, p. 1339–1360, doi:10.1016/S0278-4343(02)00010-9.

Wood, P.A., and Smith, A.J., 1958, The sedimentation and sedimentary history of the Aberystwyth Grits (Upper Llandoverian): Geological Society of London Quarterly Journal, v. 114, p. 163–195, doi:10.1144/gsjgs.114.1.0163.

Manuscript received 13 November 2013
Revised manuscript received 2 February 2014
Manuscript accepted 3 February 2014

Printed in USA